



Molecular catalysis of the oxygen reduction reaction by iron porphyrin catalysts tethered into Nafion layers: An electrochemical study in solution and a membrane-electrode-assembly study in fuel cells

Qinggang He^{a,*}, Tawanda Mugadza^b, Xiongwu Kang^c, Xiaobing Zhu^a, Shaowei Chen^c, John Kerr^a, Tebello Nyokong^b

^a Lawrence Berkeley National Laboratory, Environmental Energy Technologies Division, 1 Cyclotron Road, Berkeley, CA 94720, USA

^b Department of Chemistry, Rhodes University, P.O. Box 94, Grahamstown 6140, South Africa

^c Department of Chemistry and Biochemistry, University of California, 1156 High Street, Santa Cruz, CA 95064, USA

HIGHLIGHTS

- ▶ There exists ionic interaction between sulfonic groups of Nafion and FeTMPyP.
- ▶ The half wave potential value ($E_{1/2}$) for FeTMPyP was positively shifted by modifying the electrode with Nafion.
- ▶ Fuel cell molecular catalysis system has been demonstrated to be working based on a FeTMPyP + Nafion ionomer-coated cathode.

ARTICLE INFO

Article history:

Received 15 April 2012

Received in revised form

13 May 2012

Accepted 16 May 2012

Available online 23 May 2012

Keywords:

Non-noble metal

Iron porphyrin

Oxygen reduction reaction

Nafion

Three-dimensional catalysis

ABSTRACT

This study was motivated by the need for improved understanding of the kinetics and transport phenomena in a homogeneous catalyst system for the oxygen reduction reaction (ORR). Direct interaction between the sulfonic groups of Nafion and an Fe(III) meso-tetra(*N*-methyl-4-pyridyl) porphine chloride (Fe(III)TMPyP) compound was observed using FTIR and *in situ* UV–Vis spectroelectrochemical characterizations. A positive shift of the half wave potential value ($E_{1/2}$) for ORR on the iron porphyrin catalyst (Fe(III)TMPyP) was observed upon addition of a specific quantity of Nafion ionomer on a glassy carbon working electrode, indicating not only a faster charge transfer rate but also the role of protonation in the oxygen reduction reaction (ORR) process. A membrane electrode assembly (MEA) was made as a sandwich of a Pt-coated anode, a Nafion[®] 212 membrane, and a Fe(III)TMPyP + Nafion ionomer-coated cathode. This three-dimensional catalysis system has been demonstrated to be working in a H₂/O₂ proton exchange membrane (PEM) fuel cell test.

Published by Elsevier B.V.

1. Introduction

Widespread commercialization of proton-exchange-membrane fuel cells (PEMFCs) is dependent on its component costs and the attainment of an optimum balance between performance and durability [1,2]. In particular, the use of platinum-based electrocatalysts remains a major issue for commercial introduction due to the scarcity of platinum and price pressures due to increasing demand [3,4]. Another serious catalyst-related problem is the voltage loss resulting from sluggish kinetics at the oxygen reduction electrode. Overpotentials as large as several hundred mV, which result from poor oxygen-reduction reaction (ORR) kinetics on carbon-supported Pt catalysts, limit the rate of energy

conversion in PEMFCs [5]. The energy associated with this voltage loss is converted to heat, which must be removed through a complex heat management system that causes particular difficulties for transportation uses where the presently available radiators are inadequate.

There is, therefore, strong motivation to examine alternative, less-expensive, non-platinum catalysts that may actually perform better than platinum. Currently available non-platinum group metal (PGM) electrocatalysts can be broadly classified into pyrolyzed metal macrocycles with metal-N_x reaction centers [6–8], first-row transition metal-based chalcogenides [9–13], and electron-conducting polymer-based structures [14–16]. The so-called “acid stability” criterion has so far necessitated the transition metal reactive sites to be safely ensconced within a protective shell provided by ligands, chalcogens, etc., to prevent them from dissociation and dissolution. Non-noble transition metal-based

* Corresponding author. Tel.: +1 510 486 5433; fax: +1 510 486 7303.

E-mail addresses: QinggangHe@lbl.gov, hqma2008@gmail.com (Q. He).

(predominantly Co/Fe) monomeric phthalocyanine and porphyrin systems have been widely investigated as inexpensive electrocatalysts for oxygen reduction [17–19]. The metal atoms rather than any other part of the macrocycle are the active electrocatalytic sites whereas chelation by the ligand predominantly serves to preserve the metal atoms in the stable form for oxygen reduction [20]. Although the resulting electrodes are often highly porous with very high surface areas, the resulting catalyst layers on the electrode surface are two-dimensional in nature. With these non-platinum catalysts, the overall kinetics of oxygen reduction is much less rapid than the commercially available platinum-on-carbon electrode. It is thought that the density of the non-platinum catalytic sites is insufficient to sustain the desired reaction. With the porphyrin catalysts, for example, their poor solubility results in strong adsorption onto the carbon support with insufficient loading of the catalysts and possible deactivation of the metal centers [21–23].

Needed are electrode structures that allow an increase of the surface concentration of electrocatalysts with the activity of the catalysts fully retained. Gasteiger and co-workers [24] have provided a very thorough review of the benchmark activities required for non-Pt catalysts for oxygen reduction. Their analysis concentrated on two significant factors. The first is the turnover frequency (TOF) for the catalytic site (measured in cycles per second) and the second is the volumetric site density (measured in active sites per cm^3). The recent surge of interest in enzyme catalysts has been prompted by their potential to meet these requirements. Some earlier work has demonstrated that metal-complex systems reminiscent of enzymes appear to mimic their coordination environment [25] and proton-coupled electron-transfer process [19,26,27]. These cofacial porphyrins and related compounds not only have the basic structure of cytochrome *c* oxidase and related heme/copper terminal oxidases but also appear to be the best molecular electrocatalysts with regard to ORR yet found [28,29]. However, if the apparent benefits of enzyme catalysts [30–32] are to be realized in high-power fuel cells, then advances in catalyst design and synthesis are required to not only produce biomimetic catalysts designed for high turnover rates but also develop methods of incorporating molecular catalysts into MEAs that increase the site density to levels that can support high current densities.

One method of incorporation of such catalysts into MEAs with a sufficient site density to support high current densities lies in the attachment of the catalysts to the polymer layers that are coated on the electrode substrate particles to bind them together [33]. The work pioneered by Miller and Kerr [34,35] and further developed by Saveant, Anson, and many other workers [36–38] has demonstrated the concept of tethered redox catalysts with a basic structure of a 3-D catalyst layer. The advantage of redox catalysts lies in the three-dimensional approach of the substrates to the catalytic center as opposed to the two-dimensional approach to an electrode surface. Thus, although the rate-determining activation energy may be the same, the pre-exponential factor is much higher due to the higher frequency of collisions that occur in the three-dimensional approach of substrate to the catalyst.

A prerequisite for this concept to be highly successful is the presence of robust interactions between the redox catalysts and the ionic conductive polymers (e.g. Nafion). In addition, the ORR can benefit from the interactions with faster kinetics and without transport limitation of electrons or protons. For this purpose, in this paper, the kinetics of ORR by redox catalysts with water-soluble metalloporphyrins (Fe(III) meso-tetra(*N*-methyl-4-pyridyl) porphine chloride) in trifluoromethanesulfonic acid (TFMSA) is studied using a rotating disk electrode (RDE) coated by a Nafion film. The interaction between Fe(III)TMPyP and Nafion was examined by *in*

situ UV–vis and FTIR spectral measurements. A MEA with a cathode coated with non-pyrolyzed Fe(III)TMPyP and Nafion ionomer was developed and demonstrated in a single PEM fuel cell test.

2. Experimental section

2.1. Materials

Fe(III) meso-tetra(*N*-methyl-4-pyridyl)porphine chloride (Fe(III)TMPyP) was obtained from Frontier Scientific, Inc. Trifluoromethanesulfonic acid (TFMSA) and Nafion-alcohol solution (5%) were of analytical grade and obtained from Sigma–Aldrich. All solutions were prepared using ultrapure water from a Millipore system.

2.2. Electrochemical measurements

The electrochemical analysis was conducted in a standard three-compartment electrochemical cell using an Autolab bipotentiostat (PGSTAT302N). A glassy carbon (GC) electrode (diameter = 5.61 mm) from the Pine Instrument Company was used as the working electrode and polished with 1, 0.3, and 0.05-micron alumina slurry (Buehler, Lake Bluff, IL) successively before the experiments. For the rotating disk electrode (RDE) experiments, the GC electrode was modified with a Nafion film by the spin cast method. A Pt wire was used as the auxiliary electrode. A “No leak” Ag|AgCl reference electrode was obtained from Cypress Systems. For *in situ* UV–vis experiments, an Ag|AgCl wire pseudo-reference electrode was employed. The potential response of the Ag|AgCl pseudo-reference electrode was less than the Ag|AgCl (3 M KCl) one by 0.015 ± 0.003 V. Cyclic voltammetry (CV) and linear polarization were carried out in a three-electrode glass cell saturated with either argon or oxygen at room temperature. Electrochemical impedance spectroscopy (EIS) measurements were conducted by using an EG&G PARC Potentiostat/Galvanostat (Model 283) and Frequency Response Detector (Model 1025). The impedance spectra were recorded between 100 kHz and 10 mHz with the amplitude of the ac signal at 5 mV. Square-wave voltammetric analysis was carried out at a frequency of 10 Hz, amplitude 50 mV, and step potential 5 mV using PGSTAT302N.

2.3. *In situ* UV–vis spectroscopy

UV–vis spectra were collected with a Shimadzu UV-2550 spectrophotometer. Spectroelectrochemical data were obtained by connecting a home-made optically transparent thin-layer electrochemical (OTTLE) cell to a Bioanalytical Systems (BAS) CV 27 voltammograph. All electrochemical and spectroelectrochemical experiments were performed in trifluoromethanesulfonic acid solution (TFMSA, pH 2). Pt mesh working and auxiliary electrodes and Ag wire reference were employed for the OTTLE cell.

2.4. FTIR spectroscopy

Three samples were characterized by FTIR spectroscopy (NEXUS 670, Thermo Nicolet). Sample 1 was a GC electrode coated with 4 μm of Nafion. Sample 2 was prepared by performing 50 CV cycles [50 mV s^{-1} , -0.5 V to 0.5 V (vs. Ag/AgCl)] with Sample 1 in 0.1 M TFMSA + 0.8 mM Fe(III)TMPyP. Sample 2 was washed with ultrapure water thoroughly before collecting FTIR spectra. Sample 3 was a GC electrode coated with 180 nmol of Fe(III)TMPyP.

2.5. Catalyst ink and MEA preparation

To prepare the catalyst ink, 0.1 g Vulcan XC72R carbon powder was hydrated by several drops of isopropyl alcohol (IPA); mixed

with 0.298 g Nafion® DE2020 (20 wt.% in alkyl alcohol and water), 0.0136 g FeTMPyP, and 5 g IPA; and then horn sonicated for about 600 s. The catalyst ink was then sprayed onto four membranes to form the cathode catalyzed membrane, with a FeTMPyP loading of 0.67 mg cm^{-2} . The catalyzed membrane (cathode side), gas diffusion layer (GDL), anode Pt/C gas diffusion electrode (GDE) ($0.3 \text{ mg (Pt) cm}^{-2}$), and Nafion® NRE212 membrane were hot-pressed at 146°C for 240 s with a load of 450 kg per active 5 cm^2 MEA. For the reference Pt MEA, both anode and cathode were prepared using commercial Pt/C GDE electrodes with a Pt loading of $0.25 \text{ mg (Pt) cm}^{-2}$. The single cell was operated under H_2/O_2 at 80°C , under full humidity, $1.67 \text{ cm}^3 \text{ s}^{-1}$ of flow rate, and 68,947 Pa of back pressure.

3. Results and discussion

3.1. CV and ORR results

Cyclic voltammograms on a GC electrode coated with different amounts of Nafion in 0.1 M TFMSA + 0.8 mM Fe(III)TMPyP are shown in Fig. 1. The effect of uncompensated solution resistance (R_u) has been minimized by careful experimental design (putting the reference electrode close to the working electrode). In addition, the voltammograms for different Nafion coated electrodes were measured under the same conditions with unchanged concentration of the electrolyte and the catalyst. Also, the electrode was not rotated. So, only diffusion was counted for the transportation of catalyst from the bulk to the electrode surface. We examined the diffusion coefficient of the catalyst from the chronoamperometric (CA) measurement (not shown). The value of $1.74\text{E-}6 \text{ cm}^2 \text{ s}^{-1}$ is consistent with that reported in the literature [39] and is constant upon the changed thickness of Nafion film on the electrode. Thus, the difference due to mass transport limitations can be also ignored. In the absence of a Nafion film, a well-defined redox couple ($+0.016 \text{ V}/-0.057 \text{ V}$) corresponding to Fe(III)/Fe(II) [39,40] can be seen. It is interesting to find that the CVs exhibit larger reduction and oxidation peaks with Nafion coating up to $0.7 \mu\text{m}$ as compared to the bare electrode. This result indicates that the charge transfer through the Nafion film ($<0.7 \mu\text{m}$) to the GC electrode was actually facilitated by the presence of the Nafion film and the local density of FeTMPyP near the electrode surface may be higher than the bulk. This finding is indispensable in the sense that

the redox catalysts are required to be connected to the electrode in order to exchange electrons in the organic framework of the 3D homogeneous catalytic system [41–44]. As the mobility of metalloporphyrins has been observed to be extremely low in the Nafion film [45,46], we are inclined to believe that charge transfer between the electrode and the reaction species in solution occurred by electron hopping from one ionic site to another within the Nafion matrix [47,48]. And it implies that there must be strong interaction between the sulfonic groups of Nafion and an Fe(III)TMPyP compound. In contrast, a further increase of the Nafion film thickness results in a substantial decrease of the voltammetric peak currents along with a widening of the peak separation (ΔE_p), indicating the hindrance of the electron transfer kinetics.

As an example, the ORR curves in 0.1 M TFMSA + 0.8 mM Fe(III)TMPyP on a GC electrode coated with $0.2 \mu\text{m}$ of Nafion at different rotation rates are presented in Fig. 2. CVs recorded in argon-purged solutions at the same sweep rate were subtracted from the overall response to obtain the ORR polarization current density to minimize the influence of the reduction of metal complexes and charging of the electrode double layer. From Fig. 2, three separate regions can be identified, namely, a mixed diffusion-kinetic limited region (-0.25 V – 0.03 V) is sandwiched between a diffusion-controlled region ($E < -0.25 \text{ V}$) and a Tafel region ($E > 0.03 \text{ V}$). From the RDE data in Fig. 2, the ORR current density j can be expressed by the Koutecky–Levich equations (Eqs. (1) and (2)).

$$\frac{1}{j} = \frac{1}{j_k} + \frac{1}{j_d} + \frac{1}{j_f} \quad (1)$$

$$j_d = B\omega^{1/2} = 0.620nFD^{2/3}C_0\nu^{-1/6}\omega^{1/2} \quad (2)$$

where j_k is the kinetic current density, j_d is diffusion-limiting current density; j_f is the diffusion-limited current density through the Nafion film; n is the number of exchanged electrons; ω is the angular frequency of rotation, $\omega = 2\pi f/60$, f is RDE rotation rate in rpm; F is the Faraday constant ($96,485 \text{ C mol}^{-1}$), D is the diffusion coefficient of the molecular O_2 , ν is the kinematic viscosity, and C_0 is the concentration of molecular oxygen. In our case, the FeTMPyP catalysts were bonded with sulfonic groups and be present on the outer surface of the Nafion film. Therefore, the oxygen can be reduced without diffusion through the Nafion film. Then, the j_f can be neglected for K-L analysis.

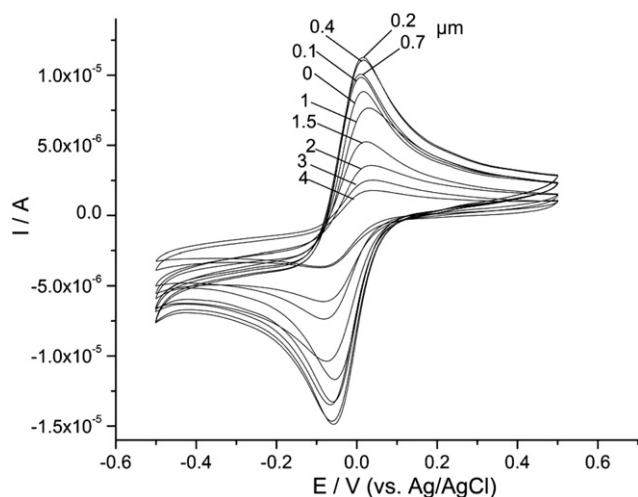


Fig. 1. Cyclic voltammograms on a glassy carbon coating with different amounts of Nafion film (marked in thickness of μm) in 0.1 M TFMSA containing 0.8 mM Fe(III) complex that was purged with argon, scan rate: 50 mV s^{-1} .

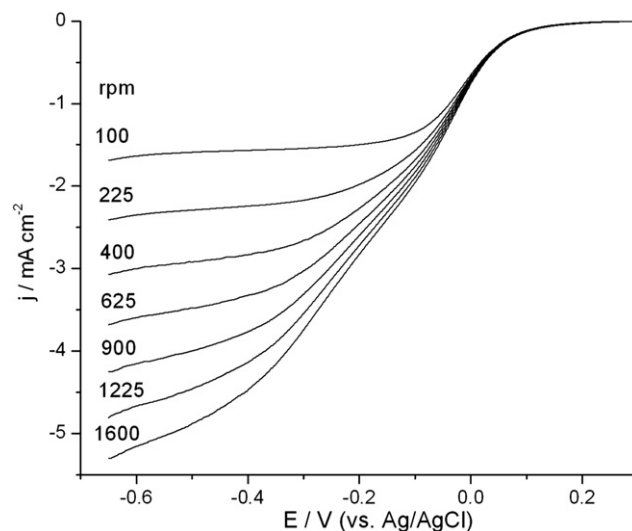


Fig. 2. Disk current density (based on the geometric area of the glassy carbon electrode) for an electrode coated with $0.2 \mu\text{m}$ of Nafion at different rotation rates during the ORR in 0.1 M TFMSA + 0.8 mM Fe(III)TMPyP. Scan rate: 20 mV s^{-1} .

Using the value of the B coefficient for O₂ reduction in 0.1 M TFMSA in the literature [49], the number of electrons transferred (*n* values) for O₂ reduction in 0.1 M TFMSA + 0.8 mM Fe(III)TMPyP on a GC electrode coated with 0.2 μm of Nafion was determined from the slope of the $1/j$ vs. $1/\omega^{1/2}$ plots, as depicted in Fig. 3. Similarly, the *n* values for different amounts of Nafion coating can be obtained and the results are listed in Table 1. It can be observed that the *n* values remained constant as 4 when the amount of Nafion on GC electrode were lower than 1 μm. In this case, the Fe(III)TMPyP is attached to the sulfonic groups of the Nafion. Once the adduct of FeP – O₂[•] is formed, the protonation state required for its activation can be easily facilitated from the protons on the nearby sulfonic groups [45,46]. Further, the complete reduction process FeP – O₂[•] → FeP + H₂O₂ → H₂O can be finished with reasonably fast electron hopping through the Nafion film [50]. In addition, the *n* values decrease generally as the amount of Nafion on the GC electrode increases. In other words, the effect of the electron transfer barrier of Nafion counteracts the proton activation effect. As a result, partial H₂O₂ cannot be further reduced to H₂O due to the sluggish electron transfer from the electrode to the catalyst active center.

Fig. 4 shows the RDE voltammograms of ORR at GC electrodes modified with different amounts of Nafion in 0.1 M TFMSA containing 0.8 mM Fe(III)TMPyP at 900 rpm. When the thickness of Nafion was smaller than 1 μm, the half-wave potentials (*E*_{1/2}) exhibited an apparent anodic shift without the onset potential change. From all *E*_{1/2} values shown in Table 1, it is clearly indicated that the coordination of Nafion with FeTMPyP may reduce the reorganization energy [51–53] of the process of O₂ + 4H⁺ + 4e → H₂O. Further coating with Nafion causes a negative shift of *E*_{1/2} and decreases the limiting current. As mentioned earlier, the diffusion of Fe(III) catalysts in Nafion is very slow. Within the experimental time domain, it is most likely that only the surface layer was contributing to the ORR currents. For coatings <1 μm, the Nafion film was porous. A further increase of the Nafion coating thickness only increased the film thickness and hence impeded the electron hopping. This Nafion-Fe(III)TMPyP system is rather complicated because the 3-D catalytic effect operates for the charge transfer process, which is driven by a chemical reaction (e.g. formation of a metal–oxygen complex). The controlling factor for

Table 1

Electrochemical kinetics parameters for ORR in 0.1 M TFMSA + 0.8 mM Fe(III)TMPyP on a glassy carbon electrode modified with different amounts of Nafion.

Nafion coating (μm) on the GC electrode	Δ <i>E</i> _p /mV	<i>E</i> _{1/2} /V (vs. Ag/AgCl) @900 rpm for the ORR	Number of electrons transferred for ORR (<i>n</i>)
0	70.6	−0.177	4.0
0.1	68.8	−0.154	4.0
0.2	73.0	−0.128	4.0
0.4	77.4	−0.142	4.0
0.7	77.1	−0.180	4.0
1	103.1	−0.221	4.0
1.5	103.0	−0.257	3.90
2	109.5	−0.307	3.82
3	111.3	−0.388	3.63
4	111.9	−0.447	3.21

this process may be either the segmental motion of the polymer for a low concentration of charge centers or a percolation mechanism for high concentrations of redox centers (Table 1).

3.2. EIS results

Electrochemical impedance spectroscopy has been used as a powerful tool in the investigation of the electron-transfer dynamics of fuel cell electrochemistry. Fig. 5a depicts the Nyquist plots of the electrochemical impedance spectra of the GC electrodes modified by varied amounts of Nafion in 0.1 M TFMSA + 0.8 mM Fe(III)TMPyP for oxygen electroreduction. The experimental data are then fitted by a modified Randles equivalent circuit shown as the Fig. 5a (inset). The variable *R*₁ represents the (uncompensated) electrolyte resistance, CPE₁ is the double-layer capacitance at the electrode–electrolyte interface where the roughness of the electrode surface may result in a deviation from a pure capacitor, *R*₂ is the charge transfer resistance, and CPE₂ denotes the Warburg-type diffusion of the redox-active species to the electrode surface. From the figure, it can be seen that the fittings (line curves) were all very good, with the results summarized in Table 2.

Upon the coating of a 0.4 μm of Nafion film on the GC electrode surface, the electrode double-layer capacitance (CPE₁) increased rather markedly to 13.4 μF from that of the naked electrode

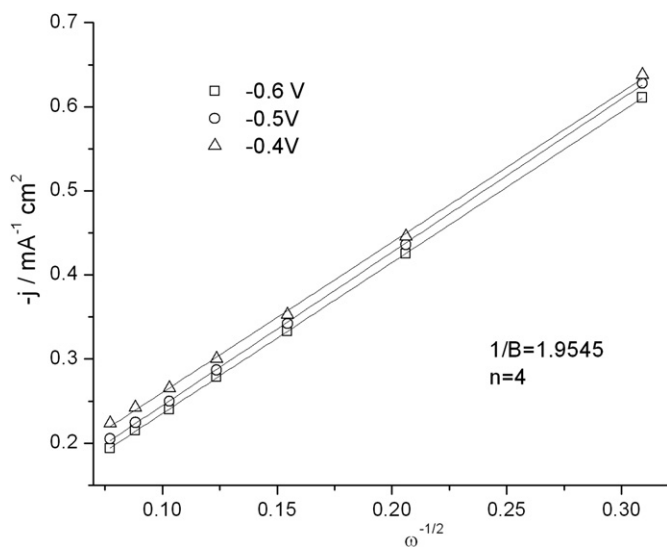


Fig. 3. Koutecky–Levich plots for oxygen reduction at different potentials in O₂-saturated 0.1 M TFMSA + 0.8 mM Fe(III)TMPyP, with 0.2 μm of Nafion on the GC electrode.

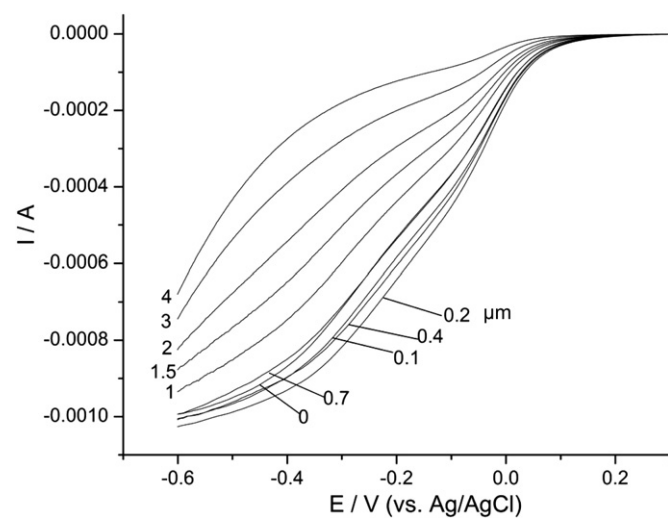


Fig. 4. Disk current density (based on the geometric area of the glassy carbon electrode) with different amount (marked in thickness of micron) of Nafion film during the ORR in 0.1 M TFMSA + 0.8 mM Fe(III)TMPyP. Rotation rate: 900 rpm, Scan rate: 20 mV s^{−1}.

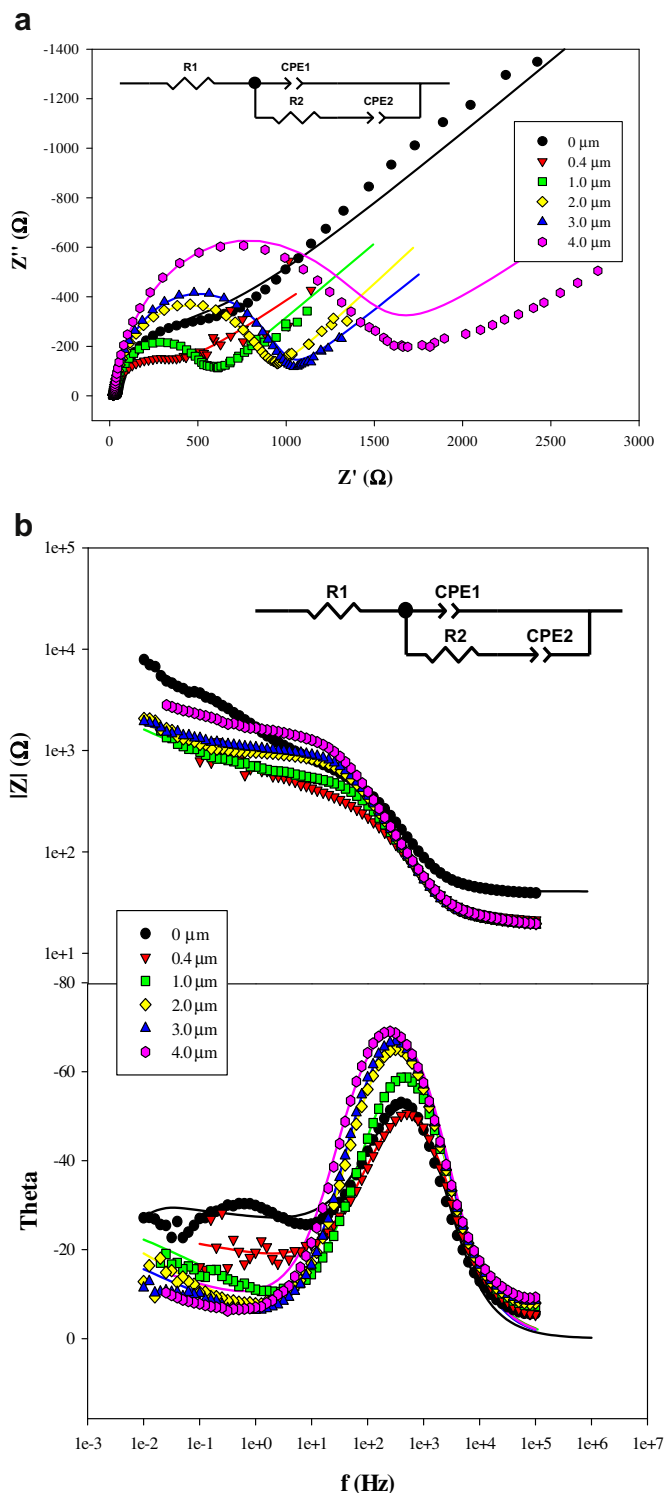


Fig. 5. (a) Nyquist plots, (b) Bode plots of the impedance spectra of the GC electrodes modified with a varied amount of Nafion (shown as figure legends) at -0.4 V (vs. Ag/AgCl) in 0.1 M TFMSA + 0.8 mM Fe(III)TMPyP for oxygen electroreduction. Symbols are experimental data and lines are the corresponding fits by the modified Randles equivalent circuit shown in the figure inset. R_1 denotes the (uncompensated) electrolyte resistance, CPE_1 is the double-layer capacitance at the electrode–electrolyte interface, R_2 is the charge transfer resistance, and CPE_2 denotes the Warburg-type impedance arising from the diffusion of redox-active species to the electrode interface.

($4.00 \mu\text{F}$), which is ascribed to the charge separation between the electrode and the Nafion film [54]. Yet with a further increase of

Table 2

Summary of the results of the fitting parameters from impedance measurements.

Coating (μm)	R_1 (Ω)	R_2 (Ω)	CPE_1 (μF)	p_1	CPE_2 (mF)	p_2
0	40.79	261.6	4.00	0.927	0.36	0.346
0.4	21.58	271.9	13.4	0.844	1.26	0.34
1	20.30	460.1	8.93	0.886	2.14	0.343
2	20.66	801.8	7.58	0.906	2.60	0.373
3	20.20	878.0	6.88	0.918	2.53	0.330
4	20.98	1232	6.55	0.914	1.12	0.289

Nafion deposition, the electrode double-layer capacitance actually exhibited an apparent decrease to, for instance, $8.93 \mu\text{F}$ at $1 \mu\text{m}$ and $6.55 \mu\text{F}$ at $4 \mu\text{m}$. It should be noted that the effective dielectric constant of Nafion is strongly dependent upon the water content [55]. Therefore, the fact that the electrode double layer capacitance reached the maximum with the deposition of $0.4 \mu\text{m}$ of Nafion onto the electrode surface seems to suggest that the water content within the Nafion layer was maximal at this coating thickness. The water might then facilitate the solvation of the Nafion film and hence the ORR electron transfer kinetics (see below). In fact, the results are consistent with those observed in Fig. 1 where the voltammetric currents due to the redox reactions of the Fe(III) complex were found to be maximal at the electrode coated with about $0.4 \mu\text{m}$ of Nafion.

Second, for CPE_2 , it can be seen that with the coating of a Nafion layer on the GC electrode surface, CPE_2 exhibited a marked increase, as compared to that at the naked electrode. This diminishment of the Warburg-type impedance indicates that the Nafion layer actually facilitated the diffusion of the proton to the electrode surface, and led to the enhancement of the catalytic performance for oxygen reduction. Furthermore, CPE_2 exhibited a peak-shaped variation with the amount of Nafion deposited onto the electrode surface, reaching the maximum within the range of 0.9 – $3 \mu\text{m}$ of Nafion. Importantly, this result suggests that the diffusion impedance was minimized at these Nafion coatings, in agreement with the above observation that hydration of the Nafion layer and hence solvation of the Fe(III) complexes was maximized with similar Nafion coatings.

Notably, for constant phase elements, when the exponential coefficient (p) is zero, it denotes actual contributions from a resistive component; at $p = 1$, it instead signifies a pure capacitor. For a pure diffusion component (e.g., the classical Warburg term), p is anticipated to be 0.5 . One may see from Table 2 that the exponential coefficients (p_2) for CPE_2 were all less than 0.5 . This behavior may be ascribed to the porous (heterogeneous) nature of the Nafion films coated on the GC electrodes, which led to frequency dispersion through the distribution of time constants along the axis normal to the 3-dimensional surface layer [56,57]. The fact that the p values fall in a narrow range implies that the degree of homogeneity of the Nafion film was similar at different Nafion loadings.

With regards to the charge transfer resistance (R_2), it can be seen that the values are all very small, ranging from 261Ω at the naked electrode to 1232Ω with the largest coating of $4 \mu\text{m}$ of Nafion, and the resistance showed a small increase with increasing thickness of the Nafion coating. In fact, Bode plots of the impedance spectra showed a decrease of the frequency at the peak of the phase angle with an increasing amount of Nafion coating on the electrode surface (Fig. 5b). This observation might be accounted for by the electron hopping process within the Nafion matrix that largely determines the electron transfer dynamics of ORR at the electrode surface.

Based on these analyses of the impacts of Nafion coating on the blocking of mass transfer as well as on the electron transfer kinetics of ORR, it can be seen that an optimal coating might be achieved with a coating of about $0.4 \mu\text{m}$.

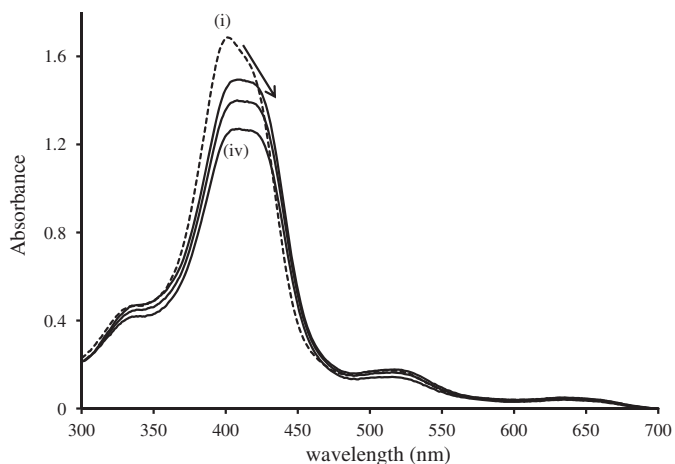


Fig. 6. UV-vis spectral changes observed for Fe(III)TMPyP in the absence (i) and presence of Nafion (ii–iv) in pH 2 TFMSA.

3.3. *In situ* UV-vis results

Fig. 6 shows the UV-Vis spectral changes observed for Fe(III)TMPyP in the absence and presence of Nafion. Upon the addition of two drops of Nafion there was a red-shift of the Soret band from 396 nm to 402 nm, and this shift was accompanied by a decrease in absorbance and band broadening [58,59]. The π - π^* transitions in metalloporphyrins are known to be affected by the complex coordination environment or by the distortion of the ring [58,59]. This red-shift could therefore be explained in terms of the interaction between Nafion with the central metal ion or with the ring, though

the latter is strongly accepted [58–60]. In the presence of Nafion, the polarity of the micro-environment decreases [60] and the metalloporphyrin complex is trapped within the Nafion interfaces [61]. This interaction causes a red-shift in the position of the Soret band and a corresponding decrease in absorbance. A further decrease in absorbance without a change in wavelength is observed upon further addition of Nafion, and this decrease could simply represent dilution of the Fe(III)TMPyP solution.

Cyclic and square-wave voltammetric studies were carried out in order to accurately determine the potentials to be applied for *in situ* UV-Vis spectroelectrochemical studies. Fig. 7 shows the observed cyclic (a) and square-wave voltammograms [b(i) and b(ii)] with three redox couples, represented as I ($E_{1/2} = -0.94$ V), II ($E_{1/2} = \sim 0.2$ V), and III ($E_{1/2} = \sim 1.3$ V). Square wave voltammetry is more sensitive relative to cyclic voltammetry and hence it was used to indicate the redox potentials more accurately. Couples I and III represent the first ring reduction and oxidation processes, respectively, while Couple II represents the Fe^{III}/Fe^{II} irreversible redox process ($\Delta E \sim 400$ mV) [62]. Spectroelectrochemical studies were conducted at slightly reductive and oxidative potentials for the established processes, Fig. 7.

Fig. 8a–c shows the observed spectral changes upon application of overpotentials to processes I, II and III, respectively. The absorption maxima are within the expected range for iron porphyrins [63]. Fig. 8a (couple I, $E_{1/2} = -0.94$ V) shows a decrease in peak intensity with no change in Soret peak position at 417 nm, representing the first ring reduction process (Fe^{II}TMPyP⁻²–Fe^{II}TMPyP⁻³). Fig. 8b shows a red-shift of the Soret band (399 nm–417 nm) and a small increase in its peak intensity upon application of slight reducing overpotentials to couple II ($E_{1/2} = \sim 0.2$ V), representing the reduction of iron (III) to iron (II) [64,65]. The presence of an isosbestic point at 405 nm is

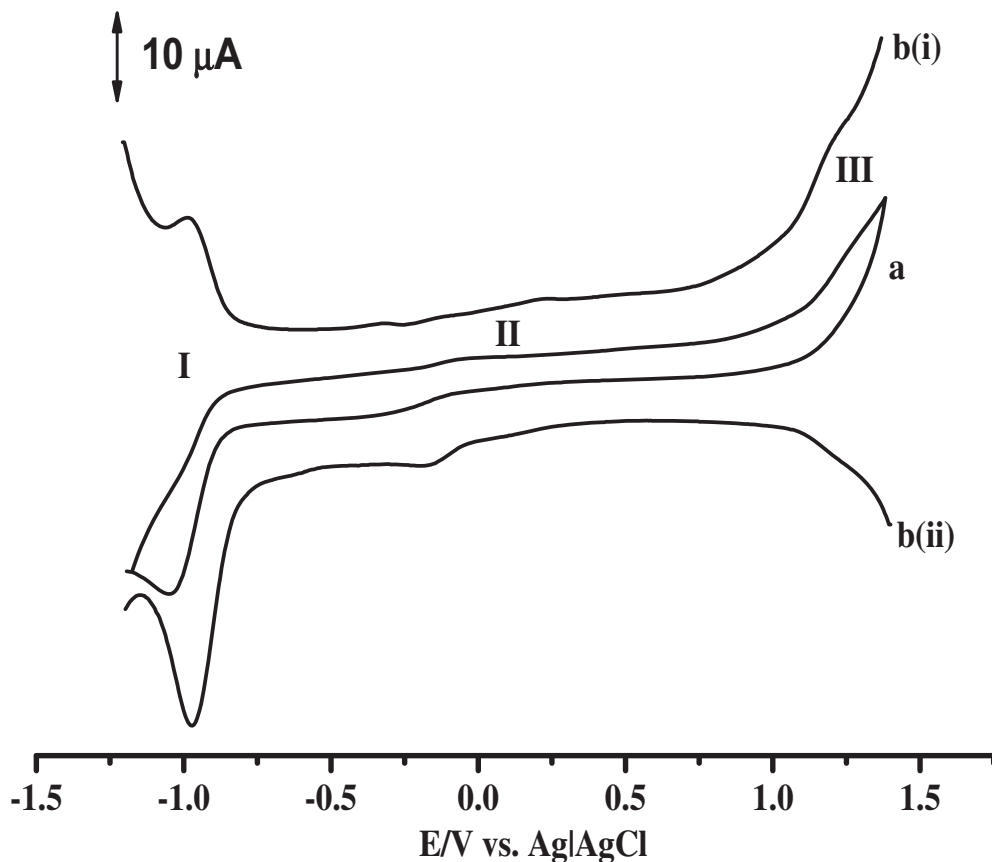


Fig. 7. Cyclic (a) and square-wave [b(i) and b(ii)] voltammograms for 0.1 mM Fe(III)TMPyP in TFMSA solution (pH 2). Scan rate: 100 mV s⁻¹.

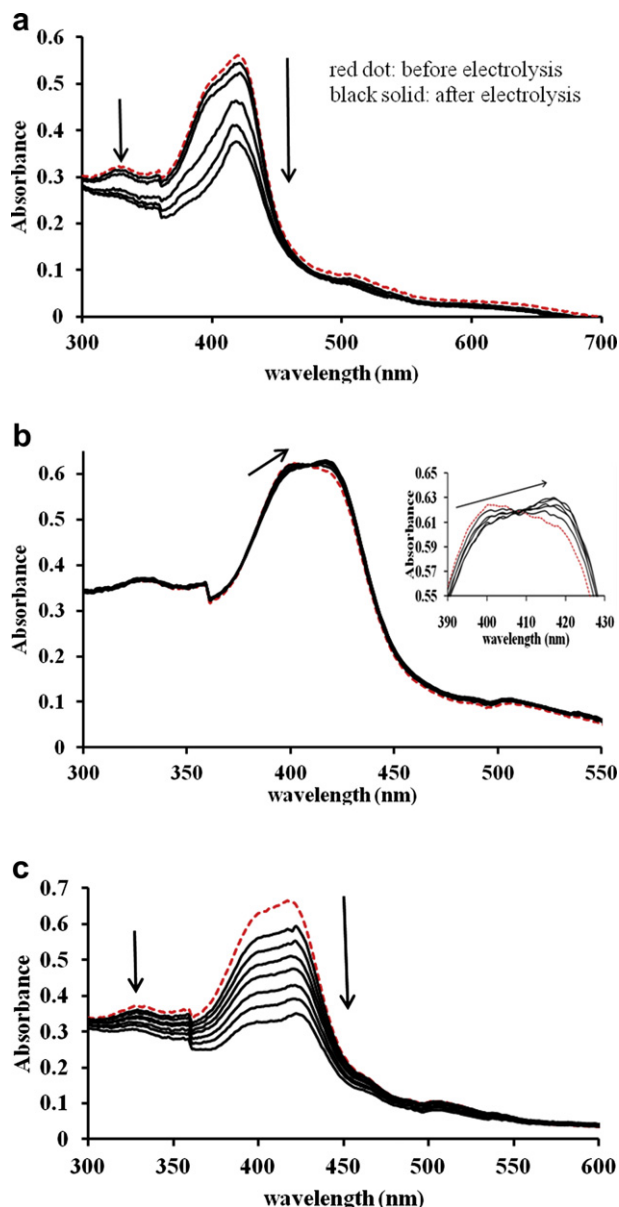


Fig. 8. UV-vis spectral changes observed in an OTLE cell for Fe(III)TMPyP during controlled-potential electrolysis for: couple I (a) $E_{1/2} = -0.94$ V, couple II (b) $E_{1/2} = \sim 0.2$ V (reduction wave): Inset, expanded view of the Soret band, and (c) $E_{1/2} = \sim 1.3$ V. All spectral studies were carried out in pH 2 TFMSA in the absence of Nafion. Dashed line (spectrum before electrolysis) and bold line (spectrum after electrolysis).

indicative of the presence of two species in solution, $\text{Fe}^{\text{III}}\text{TMPyP}$ and $\text{Fe}^{\text{II}}\text{TMPyP}$. Upon continual application of oxidative overpotentials to process III, a collapse of the Soret band at 410 nm was observed, a phenomenon that is typical of a ring-based oxidation process ($\text{Fe}^{\text{III}}\text{TMPyP}^{-1}/\text{Fe}^{\text{III}}\text{TMPyP}^{-2}$), Fig. 8c. Thus spectroelectrochemistry successfully confirmed the previous peak assignments from cyclic and square-wave voltammetric studies presented in Fig. 7.

3.4. FTIR results

Fig. 9a and b shows the ATR-FTIR spectra of Sample 1 (a GC electrode coated with Nafion film), Sample 2 (from Sample 1 after 50 CV cycles in 0.1 M TFMSA + 0.8 mM Fe(III)TMPyP), and Sample 3 (a GC electrode coated with Fe(III)TMPyP). From the spectrum of Sample 1, the vibrational absorption bands at 970 cm^{-1} and

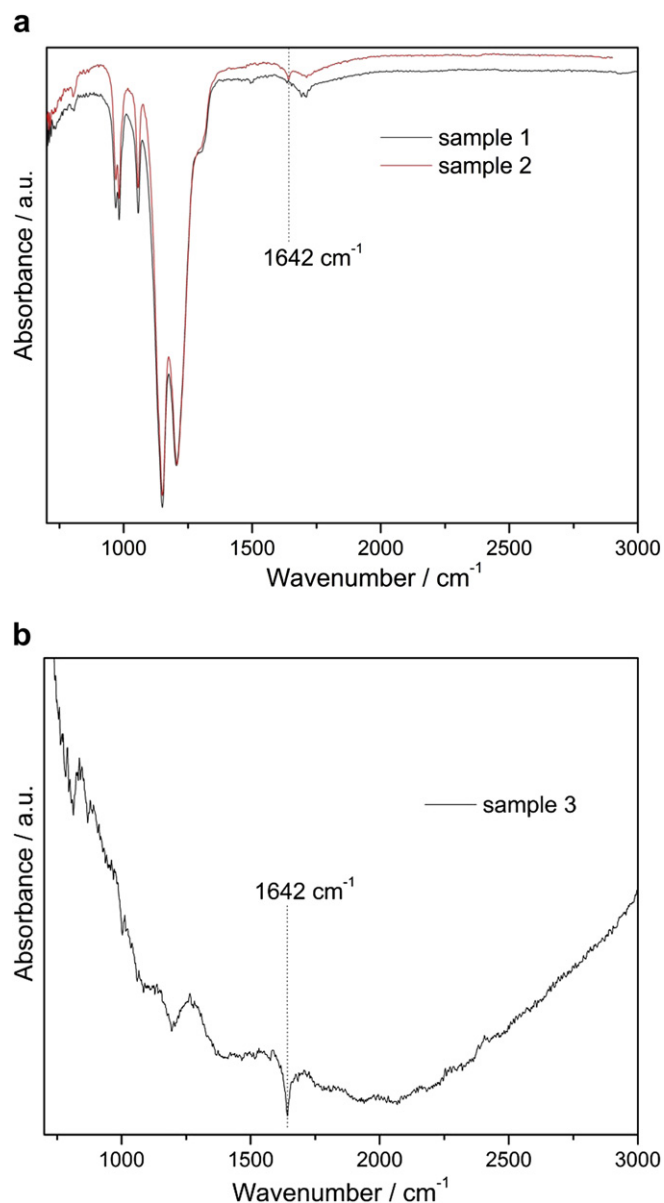


Fig. 9. a. ATR-FTIR spectrum of Sample 1 (GC electrode coated with Nafion) and Sample 2 (from Sample 1 after adsorption of Fe(III)TMPyP). b. ATR-FTIR spectrum of Sample 3 (GC electrode coated with Fe(III)TMPyP).

985 cm^{-1} (ether linkage), 1057 cm^{-1} (S–O symmetric stretching), 1148 cm^{-1} and 1203 cm^{-1} (CF_2 group stretching), and 1304 cm^{-1} (C–C symmetric stretching) are consistent with those reported in the literature [66,67]. Clearly, after incorporation of Fe(III)TMPyP into the Nafion, Sample 2 shows an extra peak at 1642 cm^{-1} that corresponds to the vibration of porphyrin [65]. Fig. 9b is the FTIR spectrum of Fe(III)TMPyP on a GC electrode, which also shows an identical peak at 1642 cm^{-1} . Based on the above information, one can conclude that there is ionic interaction between Fe(III)TMPyP and Nafion. A reasonable hypothesis is that the positively charged pyridine groups and metal iron center in Fe(III)TMPyP are attracted by the negatively charged sulfonic groups in Nafion and a composite can be formed due to an electrogenic effect. In addition, bonding may also be aided by the similar hydrophilicity of the sulfonic groups in Nafion and Fe(III)TMPyP. Nevertheless, a subtle change of S–O symmetric stretching band at 1057 cm^{-1} can be observed for Sample 2 as compared to

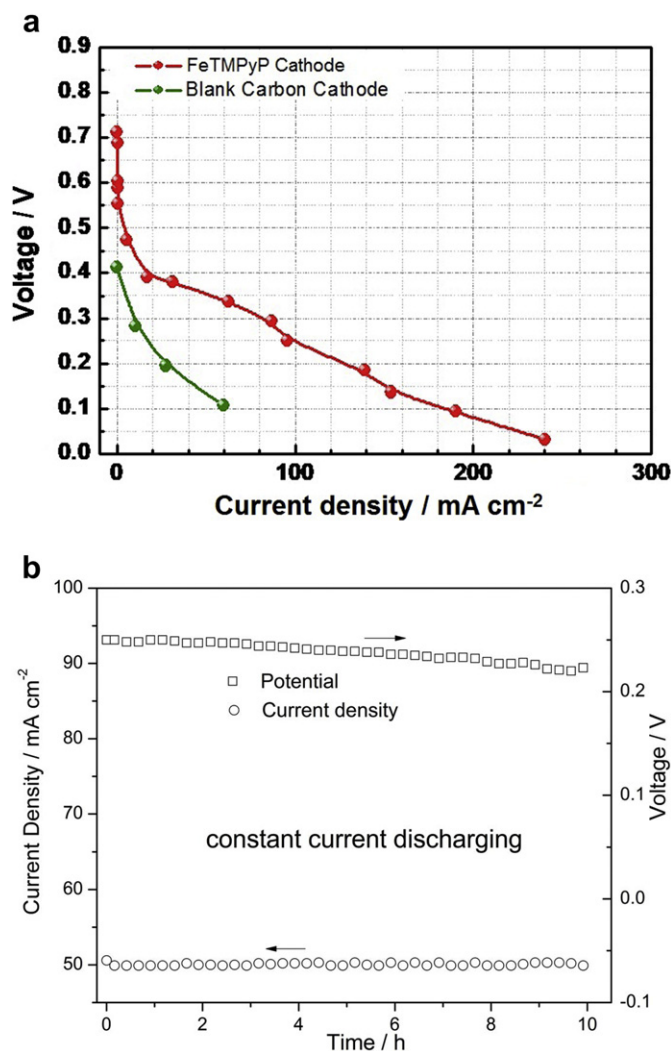


Fig. 10. a. Polarization curves of fuel cells employing commercial Pt/C GDE anode, and varied cathodes, under H_2/O_2 at 80°C full humidity, 1.67 and $3.34\text{ cm}^3\text{ s}^{-1}$, and $68,947$ and $1,034,205\text{ Pa}$ for anode and cathode flow rate, and back pressure, respectively. The red and dark green curves represent a Fe(III)TMPyP cathode and a blank carbon cathode. b. Ten hours durability testing of single fuel cell employing non-PGM molecular catalyst cathode using FeTMPyP Cl_5 catalyst with loading of $0.67\text{ mg}_{\text{cat}}\text{ cm}^{-2}$ under conditions of H_2/O_2 at 80°C full humidity, 1.67 and $3.34\text{ cm}^3\text{ s}^{-1}$, and $68,947$ and $1,034,205\text{ Pa}$ for anode and cathode flow rate, and back pressure, respectively. (For interpretation of the references to colour in this figure legend, the reader is referred to the web version of this article.)

Sample 1. This change may be attributed to the extremely low amount of Fe(III)TMPyP attached in the Nafion matrix.

3.5. MEA results

It is shown in Fig. 10a that a Fe(III)TMPyP cathode exhibits a higher open circuit voltage (OCV) at 0.712 V , as compared to the blank carbon at 0.4 V . Its short-circuit current density reaches 240 mA cm^{-2} , indicating successful demonstration of the molecular catalysis concept in MEAs for fuel cell ORR catalysis. Relative to commercial Pt/C cathode developed decades ago, the development of the electrode structure for the molecular catalysis in fuel cells is in its very “early” stage and will require improvements to achieve favorable or competitive fuel cell performance. Subsequently, it is essential to improve the electrode structure by adjusting the geometry to optimize the triple phase boundaries, opening

ionomer ionic clusters to enhance the connection possibility to the reaction center, and tuning the interface between polymer and carbon. Fig. 10b shows 10 h durability testing of single fuel cell employing non-PGM molecular catalyst cathode using FeTMPyP catalyst with loading of $0.67\text{ mg}_{\text{cat}}\text{ cm}^{-2}$. It demonstrated that the single cell voltage drop rate value was 2.7 mV h^{-1} under constant current discharging at 50 mA cm^{-2} , although the potential value was low due to its lower initial performance.

4. Conclusions

The kinetic parameters and catalytic activity for a homogeneous catalysis system of iron porphyrin (Fe(III)TMPyP) coordinated with Nafion were examined as a potential ORR electrode in acid media. Ionic interaction between sulfonic groups of Nafion and Fe(III)TMPyP was proved by FTIR and *in situ* UV–vis measurements. With the above effect, an interesting positive shift of the $E_{1/2}$ value for the ORR in $0.1\text{ M TFMSA} + 0.8\text{ mM Fe(III)TMPyP}$ was observed when modifying the glassy carbon electrode with Nafion ionomer. On the basis of EIS measurements, the shift of the $E_{1/2}$ value can be attributed to faster kinetics for charge transfer. Finally, a MEA with Pt/C anode, Nafion 212 separator and a Nafion and Fe(III)TMPyP mixture coated cathode was tested in a H_2/O_2 fuel cell. It is encouraging for the molecular catalysis electrode to show maximum/short circuit current density of 240 mA cm^{-2} and degradation rate of 2.7 mV h^{-1} under constant current discharging at 50 mA cm^{-2} . Further improved performance can be expected with more active catalysts, alternative ionomers (e.g. lower equivalent weight ionomers with more sulfonic acid groups) and optimized electrode structure.

Acknowledgement

This work was supported by the Assistant Secretary for Energy Efficiency and Renewable Energy, Office of Hydrogen, Fuel Cells and Infrastructure Technologies of the U.S. Department of Energy under Contract No. DE-AC02-05CH11231. We would like to thank Dr. Nicholas Norberg for the assistance of FTIR measurements. We also thank Dr. Frank McLaren for helpful comments and suggestions during preparation of this manuscript.

References

- [1] B.C.H. Steele, A. Heinzel, *Nature* 414 (2001) 345–352.
- [2] J. Xie, D.L. Wood III, K.L. More, P. Atanassov, R.L. Borup, *J. Electrochem. Soc.* 152 (2005) A1011–A1020.
- [3] G. Brumfiel, *Nature* 422 (2003) 104.
- [4] D.J. Berger, *Science* 286 (1999) 49.
- [5] V.S. Murthi, R.C. Urian, S. Mukerjee, *J. Phys. Chem. B* 108 (2004) 11011–11023.
- [6] Q. He, X. Yang, X. Ren, B.E. Koel, N. Ramaswamy, S. Mukerjee, R. Kostecki, *J. Power Sources* 196 (2011) 7404–7410.
- [7] Z.P. Li, B.H. Liu, *J. Appl. Electrochem.* 40 (2010) 475–483.
- [8] S. Pylypenko, S. Mukherjee, T.S. Olson, P. Atanassov, *Electrochim. Acta* 53 (2008) 7875–7883.
- [9] D. Susac, A. Sode, L. Zhu, P.C. Wong, M. Teo, D. Bizzotto, K.A.R. Mitchell, R.R. Parsons, S.A. Campbell, *J. Phys. Chem. B* 110 (2006) 10762–10770.
- [10] L. Zhu, D. Susac, A. Lam, M. Teo, P.C. Wong, D. Bizzotto, S.A. Campbell, R.R. Parsons, K.A.R. Mitchell, *J. Solid State Chem.* 179 (2006) 3942–3948.
- [11] R.A. Sidik, A.B. Anderson, *J. Phys. Chem. B* 110 (2006) 936–941.
- [12] E. Vayner, R.A. Sidik, A.B. Anderson, B.N. Popov, *J. Phys. Chem. C* 111 (2007) 10508–10513.
- [13] Y. Feng, T. He, N. Alonso-Vante, *Chem. Mater.* 20 (2008) 26–28.
- [14] R. Bashyam, P. Zelenay, *Nature* 443 (2006) 63–66.
- [15] V.G. Khomenko, V.Z. Barsukov, A.S. Katashinskii, *Electrochim. Acta* 50 (2005) 1675–1683.
- [16] M. Yuasa, H. Murata, K. Ikkanda, K. Tanaka, T. Imai, K. Oyaizu, *Mater. Technol.* 25 (2007) 313–319.
- [17] R.J. Jasinski, *Nature* 201 (1964) 1212–1213.
- [18] Y. Kiros, *Int. J. Electrochem. Sci.* 2 (2007) 285–300.
- [19] C.J. Chang, Z.-H. Loh, C. Shi, F.C. Anson, D.G. Nocera, *J. Am. Chem. Soc.* 126 (2004) 10013–10020.

- [20] P. Vasudevan, Santosh, N. Mann, S. Tyagi, *Transit. Met. Chem.* 15 (1990) 81–90.
- [21] Y. Ji, Z. Li, S. Wang, G. Xu, X. Yu, *Int. J. Hydrogen Energy* 35 (2010) 8117–8121.
- [22] J.A.R. Van Veen, H.A. Colijn, *Ber. Bunsen Ges. Phys. Chem.* 85 (1981) 700–704.
- [23] J.A.R. Van Veen, J.F. Van Baar, C.J. Kroese, J.G.F. Coolegem, N. De Wit, H.A. Colijn, *Ber. Bunsen Ges. Phys. Chem.* 85 (1981) 693–700.
- [24] H.A. Gasteiger, S.S. Kocha, B. Sompalli, F.T. Wagner, *Appl. Catal. B* 56 (2005) 9–35.
- [25] J.P. Collman, N.K. Devaraj, R.A. Decreau, Y. Yang, Y.-L. Yan, W. Ebina, T.A. Eberspacher, C.E.D. Chidsey, *Science* 315 (2007) 1565–1568.
- [26] C.J. Chang, L.L. Chng, D.G. Nocera, *J. Am. Chem. Soc.* 125 (2003) 1866–1876.
- [27] C.J. Chang, Y. Deng, D.G. Nocera, C. Shi, F.C. Anson, C.K. Chang, *Chem. Commun.* (2000) 1355–1356.
- [28] J.P. Collman, R. Boulatov, C.J. Sunderland, in: K.M. Kadish, K.M. Smith, R. Guilard (Eds.), *The Porphyrin Handbook*, Academic Press, Boston, 2003.
- [29] J.P. Collman, P.S. Wagenknecht, J.E. Hutchison, *Angew. Chem. Int. Ed.* 33 (1994) 1525–1674.
- [30] J.A. Cracknell, K.A. Vincent, F.A. Armstrong, *Chem. Rev.* 108 (2008) 2439–2461.
- [31] E. Vayner, H. Schweiger, A.B. Anderson, *J. Electroanal. Chem.* 607 (2007) 90–100.
- [32] H. Schweiger, E. Vayner, A.B. Anderson, *Electrochem. Solid State Lett.* 8 (2005) A585–A587.
- [33] J.-M. Saveant, *Chem. Rev.* 108 (2008) 2111–2112.
- [34] J.B. Kerr, L.L. Miller, M.R. Van de Mark, *J. Am. Chem. Soc.* 102 (1980) 3383–3390.
- [35] J.B. Kerr, L.L. Miller, *J. Electroanal. Chem. Interfacial Electrochem.* 101 (1979) 263–267.
- [36] F.C. Anson, C.L. Ni, J.M. Saveant, *J. Am. Chem. Soc.* 107 (1985) 3442–3450.
- [37] C.P. Andrieux, C. Blocman, J.M. Dumas-Bouchiat, J.M. Saveant, *J. Am. Chem. Soc.* 101 (1979) 3431–3441.
- [38] C.P. Andrieux, O. Haas, J.M. Saveant, *J. Am. Chem. Soc.* 108 (1986) 8175–8182.
- [39] P.A. Forshey, T. Kuwana, *Inorg. Chem.* 20 (1981) 693–700.
- [40] T. Kuwana, M. Fujihira, K. Sunakawa, T. Osa, *J. Electroanal. Chem. Interfacial Electrochem.* 88 (1978) 299–303.
- [41] F. Jaouen, F. Charreter, J.P. Dodelet, *J. Electrochem. Soc.* 153 (2006) A689–A698.
- [42] D. Villers, X. Jacques-Bedard, J.-P. Dodelet, *J. Electrochem. Soc.* 151 (2004) A1507–A1515.
- [43] M. Lefevre, J.P. Dodelet, P. Bertrand, *J. Phys. Chem. B* 109 (2005) 16718–16724.
- [44] S. Marcotte, D. Villers, N. Guillet, L. Roue, J.P. Dodelet, *Electrochim. Acta* 50 (2004) 179–188.
- [45] G.V. Zhutavaeva, M.R. Tarasevich, M.V. Radina, I.S. Chernyshova, *Russ. J. Electrochem.* 45 (2009) 1080–1088.
- [46] M.R. Tarasevich, A. Sadkovsky, E. Yeager, in: B.E. Conway, J.O.M. Bockris, E. Yeager, S.U.M. Kahn, R.E. White (Eds.), *Comprehensive Treatise of Electrochemistry*, vol. 7, Plenum Publ. Corp, New York, 1983.
- [47] D.N. Blauch, J.M. Saveant, *J. Am. Chem. Soc.* 114 (1992) 3323–3332.
- [48] D.N. Blauch, J.M. Saveant, *J. Phys. Chem.* 97 (1993) 6444–6448.
- [49] P.N. Ross, P.C. Andricacos, *J. Electroanal. Chem. Interfacial Electrochem.* 154 (1983) 205–215.
- [50] F.C. Anson, D.N. Blauch, J.M. Saveant, C.F. Shu, *J. Am. Chem. Soc.* 113 (1991) 1922–1932.
- [51] J.M. Calvert, D.L. Peebles, R.J. Nowak, *Inorg. Chem.* 24 (1985) 3111–3119.
- [52] K. Kumar, F.P. Rotzinger, J.F. Endicott, *J. Am. Chem. Soc.* 105 (1983) 7064–7074.
- [53] B. Durham, J.F. Endicott, C.-L. Wong, D.P. Rillema, *J. Am. Chem. Soc.* 101 (1979) 847–857.
- [54] C.M.A. Brett, V.A. Alves, D.A. Fungaro, *Electroanalysis* 13 (2001) 212–218.
- [55] S.J. Paddison, D.W. Reagor, T.A. Zawodzinski, *J. Electroanal. Chem.* 459 (1998) 91–97.
- [56] E. Barsoukov, J.R. Macdonald, *Impedance Spectroscopy: Theory, Experiment, and Applications*, second ed. Wiley-Interscience, Hoboken, NJ, 2005.
- [57] M.E. Orazem, B. Tribollet, *Electrochemical Impedance Spectroscopy*, Wiley, Hoboken, NJ, 2008.
- [58] T. Kuwabara, M. Yagi, *J. Phys. Chem. B* 110 (2006) 14673–14677.
- [59] A.L. Maclean, R.S. Armstrong, B.J. Kennedy, *J. Raman Spectrosc.* 24 (1993) 897–901.
- [60] V.V. Vasil'ev, S.M. Borisov, A. Maldotti, A. Molinari, *J. Porphyrins Phthalocyanines* 7 (2003) 780–786.
- [61] R. Czolk, *Sens. Actuators, B: Chem.* B30 (1996) 61–63.
- [62] J. Lei, H. Ju, O. Ikeda, *J. Electroanal. Chem.* 567 (2004) 331–338.
- [63] Z. Wei, M.D. Ryan, *Inorganica Chim. Acta* 314 (2001) 49–57.
- [64] J.H. Cameron, S.C. Turner, *Polyhedron* 12 (1993) 1675–1680.
- [65] J. Chen, O. Ikeda, T. Hatasa, A. Kitajima, M. Miyake, A. Yamatodani, *Electrochem. Commun.* 1 (1999) 274–277.
- [66] Y. Itagaki, S. Nakashima, Y. Sadaoka, *Sen. Actuators B: Chem.* B142 (2009) 44–48.
- [67] N. Ramaswamy, N. Hakim, S. Mukerjee, *Electrochim. Acta* 53 (2008) 3279–3295.